JACS Au
AN OPEN ACCESS JOURNAL OF THE AMERICAN CHEMICAL SOCIETY

pubs.acs.org/jacsau

Article

Cage$^-$···Cage$^-$ Interaction: Boron Cluster-Based Noncovalent Bond and Its Applications in Solid-State Materials

Deshuang Tu, Jiaxin Li, Fangxiang Sun, Hong Yan,* Jordi Poater,* and Miquel Solà*

Cite This: *JACS Au* 2021, 1, 2047−2057

Read Online

ACCESS | Metrics & More | Article Recommendations | Supporting Information

ABSTRACT: Carboranes are boron−carbon clusters with important applications in the fields of materials, catalysis, pharmaceuticals, etc. However, the noncovalent interactions that could determine the solid-state structures and properties of such boron clusters have rarely been investigated. Herein, inspired by the coordinate bond in metallacarborane or ferrocene, the boron cluster-based noncovalent interaction (denoted as cage$^-$···cage$^-$ interaction) between two *nido*-carborane clusters was successfully realized by using a pyridinium-based molecular barrier. The X-ray diffraction studies uncover that the cage$^-$···cage$^-$ interaction has a contacting distance of 5.4−7.0 Å from centroid to centroid in the systems reported here. Theoretical calculations validate the formation of the noncovalent interaction and disclose its repulsive bonding nature that is overcome thanks to the positively charged pyridinium-based framework. Interestingly, such bulk crystalline materials containing the cage$^-$···cage$^-$ interaction show relevant properties such as full-color absorption in the visible light range and important photothermal effect, which are absent for the control compound without carboranes. This study may offer fundamental insights into the boron cluster-based noncovalent interactions and open a new research avenue to rationally design boron cluster-based materials.

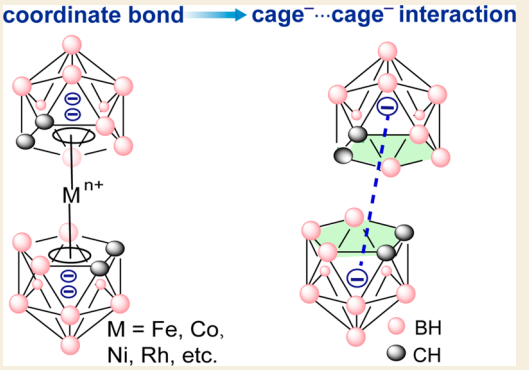

KEYWORDS: *boron clusters, noncovalent interaction, carborane, energy decomposition analysis, aromaticity, photothermal effect*

INTRODUCTION

Carboranes are a class of polyhedral boron−carbon molecular clusters.[1] As one of the famous families of boron clusters, carboranes have been extensively studied because of the important applications of their derivatives in the fields of functional materials, catalysis, pharmaceuticals, etc.[2−10] For example, through tailoring the structures, carboranes can undergo efficient photo/electroluminescence, thus showing excellent performances in luminescent materials and fluorescent sensors.[11−14] In addition, carboranes as pharmacophores have also been developed for medicinal applications such as in boron neutron capture therapy (BNCT).[15−19] Despite these known important investigations, a comprehensive understanding of the structure−property relationship has not been fully established yet[20,21] because of the lack of research concerning noncovalent interactions for these polyhedral boranes.

As three-dimensional analogs of aromatic rings, carboranes have unique structural features like bulk-size-cage geometry, delocalization of the skeletal electrons through multicenter two-electron bonds, and three-dimensional global aromaticity.[22−28] All these render carboranes with different attributes compared to planar aromatic rings (Figure 1a). Even though the noncovalent interactions involved in two-dimensional aromatic species are ubiquitous and play vital roles in many important chemical and biological processes,[29−37] those based on carborane moieties have been seldom studied, except B−H···π, B−H···H−B, and other related interactions.[38−47] In particular, the noncovalent interaction generated by two three-dimensional and negatively charged aromatic carborane moieties is unknown to date.

Herein, inspired by the coordinate bond in transition metal complexes[48] (Figure 1b, left), the cationic pyridinium-based molecular barrier is used to obtain the boron cluster-based cage$^-$···cage$^-$ interaction (Figure 2). This unique noncovalent interaction could be validated in carborane derivatives with a contacting distance of 5.4−7.0 Å from centroid to centroid. Theoretical calculations also clarified the formation of such cage$^-$···cage$^-$ interaction, and disclosed its repulsive bonding nature, which is not the same as that of the known π···π bond. Moreover, such cage$^-$···cage$^-$ interaction-constructed bulk crystalline materials showed interesting photophysical and electrical properties such as the red-shift charge transfer

Received: August 11, 2021
Published: October 8, 2021

https://doi.org/10.1021/jacsau.1c00348
JACS Au 2021, 1, 2047−2057

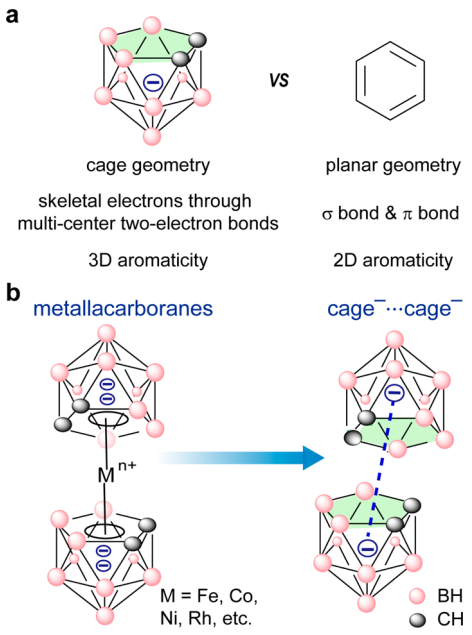

Figure 1. (a) Differences between *nido*-carborane and benzene. (b) Noncovalent interaction is formed between two *nido*-carboranes (right). *nido*-$C_2B_9H_{10}^{2-}$ was used as a ligand to form stable complexes (left). Hydrogen atoms of the molecules are omitted for clarity. The pink ball represents the BH unit, whereas the gray ball represents the CH unit.

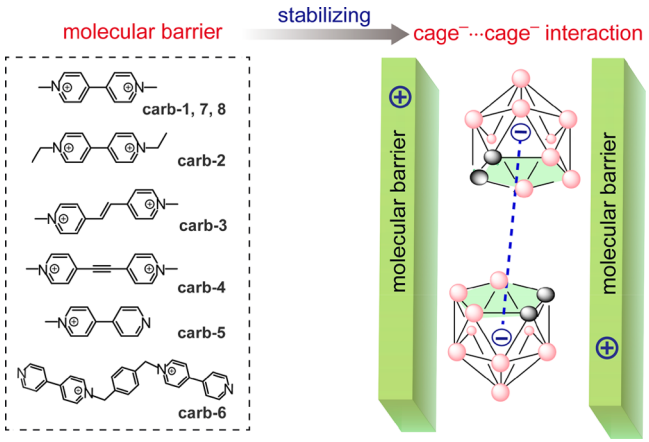

Figure 2. Cage⁻···cage⁻ interaction in boron clusters. This noncovalent bond is generated when *nido*-carborane units are surrounded by pyridinium units, which are used as molecular barriers to hold the two negatively charged *nido*-carboranes. Hydrogen atoms of the molecules are omitted for clarity. The pink ball represents the BH unit, whereas the gray ball represents the CH unit.

absorption in the crystalline state, the enhanced electrical conductivity in bulk crystals, and the efficient photothermal conversion (vide infra). Therefore, this study not only reports a boron cluster-based noncovalent interaction but also explores its bonding nature and potential applications.

RESULTS AND DISCUSSION

Molecular Design and Synthesis

It is well-known that the three-dimensional *nido*-carborane possesses a cage structure and partially negatively charged B–H bonds. These structural features may give rise to an easy packing arrangement between the *nido*-carborane and different counterions.[47] Thus, the cage⁻···cage⁻ interaction is hardly realized because of both strong Coulomb repulsion and large steric hindrance. This is also proven by a search of all the crystal structures containing the *nido*-carborane unit in the Cambridge Crystallographic Data Centre (CCDC) database. No such cage⁻···cage⁻ interaction with close contact of B/C···B/C (Figure 3b) could be found, except cage···π,[47] B–H···π,[38,39] or B–H···H–B[41] interactions (Figure S1). In this regard, it remains a challenge to obtain a noncovalent bond between two large-sized and aromatic boron cluster anions with close proximity.

On the other hand, chemical bonds are present when the bonding atoms are in thermodynamically stable or metastable assemblies.[49,50] As revealed in coordination chemistry, a coordinate bond is generated if an electron-deficient metal center meets an electron-rich ligand. Such a binding interaction enables it to overcome the repulsive interactions from other anionic ligands in the coordinative sphere, which ultimately leads to the formation of stable complexes such as ferrocene and metallacarboranes (Figure 1b, left).[51] This inspired us to design such an arrangement where two negatively charged *nido*-carboranes are placed together (see Figure 1b, right) by the use of a positively charged but larger organic counterion, instead of a metallic atom, as demonstrated in Figure 2 to balance the electronic repulsion, driving to the formation of an intermolecular interaction involving two boron clusters. We are aware of the existence of many examples of supramolecular systems that stabilize two or more like-charged species such as F^-, Cl^-, Br^-, SO_4^{2-}, HCO_3^-, or $H_2PO_4^-$, among others.[52−61] However, if stabilized, the proposed cage⁻···cage⁻ interaction would represent a unique type of anion···anion interaction.

To validate the above hypothesis, we designed positively charged structural units of π-based frameworks[52] (Figure 2, left). Because of the attractive interaction between a cationic molecular barrier and *nido*-carborane anion, the electrostatic repulsion between the two *nido*-carboranes could be counterbalanced. Besides, the π-based framework could provide a tailorable molecular topology, which may devote to the formation of a matched molecular barrier with a specific confined space to stabilize such a repulsive noncovalent interaction. Herein, the rational design of the template of molecular barrier to form a cage⁻···cage⁻ interaction on the basis of *nido*-carborane is presented for the first time.

The *nido*-carborane-based compounds were synthesized by ion exchange in high yields (Schemes S1–S4). The success of the ion exchange reaction also supports the attractive interaction between the bipyridinium-based cation and the *nido*-carborane anion. These complexes were carefully characterized by ^{1}H-, ^{13}C-, ^{11}B-NMR, and X-ray diffraction (Table S1, Figure S2).

Structure Analysis of Cage⁻···Cage⁻ Interaction

The crystal packing structures of these compounds are shown in Figures 3 and 4 and Figures S3–S10. As expected, the pyridinium systems determine the crystal packing structures, particularly for the interaction between the two *nido*-carboranes. For compound **carb-1**, the two *nido*-carboranes are surrounded by multiple pyridinium cations (Figure S3a). With careful inspection, a sandwich-type packing conformation between two *nido*-carboranes and two pyridiniums was observed (Figure 3a and Figure S3, note that some of the *nido*-carborane anions in Figures 3 and 4 were omitted in the

https://doi.org/10.1021/jacsau.1c00348
JACS Au 2021, 1, 2047−2057

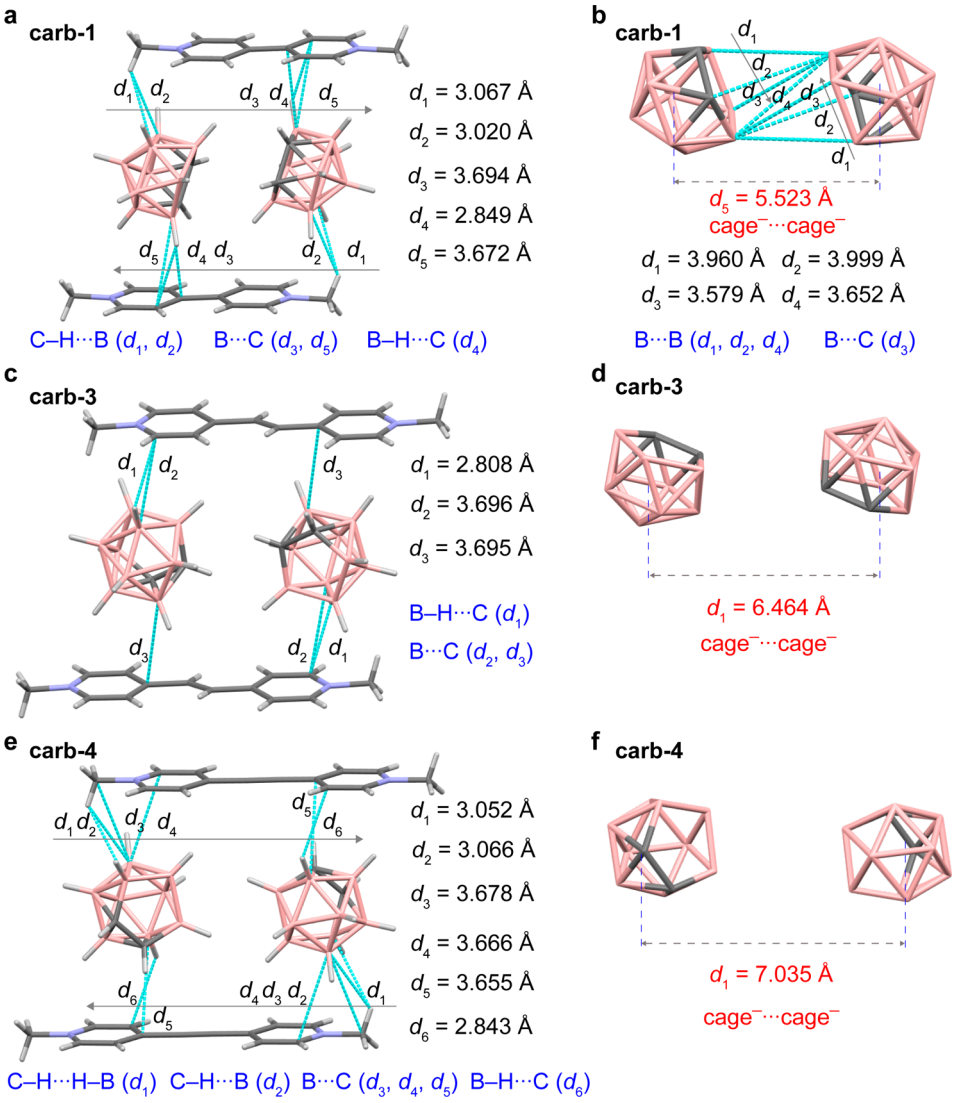

Figure 3. Crystal packing structures of *nido*-carborane-based compounds with different cationic frameworks (blue, nitrogen; dark gray, carbon; pink, boron; light gray, hydrogen). The contacting distances of the noncovalent bonds are indicated with light blue/black dashed lines. Some hydrogen atoms have been omitted for clarity.

crystal packing structures for clarity), which is reminiscent of the coordinative bond in metallacarboranes. As a consequence, the formed multiple intermolecular contacts such as C−H···B and B−H···C interactions should devote to stabilizing the repulsive interaction between the two *nido*-carboranes (Figure 2 and Figure S3a). The cation-based framework seems to create a molecular barrier (Figure 2 and Figure S3) to provide a confined space, thus holding *nido*-carboranes together and leading to the cage$^-$···cage$^-$ interaction with a distance of 5.523 Å (centroid to centroid, Figure 3b). Interestingly, the two C_2B_3 rings from two *nido*-carboranes adopt an antisymmetric and parallel displaced geometry with a B···B/C contact of 3.579−3.999 Å (Figure 3b) below the sum of van der Waals radii (r_B = 1.92 Å, r_C = 1.70 Å).[62] This further demonstrates the close contact of two boron clusters, similar to the packing mode of a π···π bond as found in two-dimensional aromatic systems.[63]

Next, effect of the variation in pyridinium on the supramolecular assembly was examined. If the molecular barrier is lengthened by adding one double bond or one triple bond or even replacing the methyl of pyridinium with an ethyl as shown in compounds **carb-2**−**4** (Figures 3c−f and Figure S4−S6), the longer distances of the cage$^-$···cage$^-$ interaction (6.464−7.035 Å) were observed. The close contact of parallel-displaced C_2B_3···C_2B_3 units in **carb-1** disappears, although the confined space triggered by the molecular barrier and the formed multiple intermolecular interactions like B−H···C or B−H···H−C interactions are still present in **carb-2**−**4**. This suggests that holding two *nido*-carboranes in close contact is not easy to achieve because of the repulsive interaction and the bulky cage structure. Namely, if the *nido*-carborane is attached to a nonmatched molecular barrier, the attractive interactions between the *nido*-caborane moiety and the π-based molecular barrier based on multiple B−H···C and/or C−H···B non-covalent bonds and others cannot overcome the liability of the repulsive cage$^-$···cage$^-$ interaction in the crystalline state (Figure 3). This directly leads to a longer contacting distance of cage$^-$···cage$^-$ interaction. Obviously, a matched molecular barrier is crucial for the realization of the interaction between two *nido*-carboranes.

To further demonstrate that the parallel-displaced cage$^-$··· cage$^-$ interaction with close proximity can be tuned by a cationic molecular barrier, we designed and synthesized more

https://doi.org/10.1021/jacsau.1c00348
JACS Au 2021, 1, 2047−2057

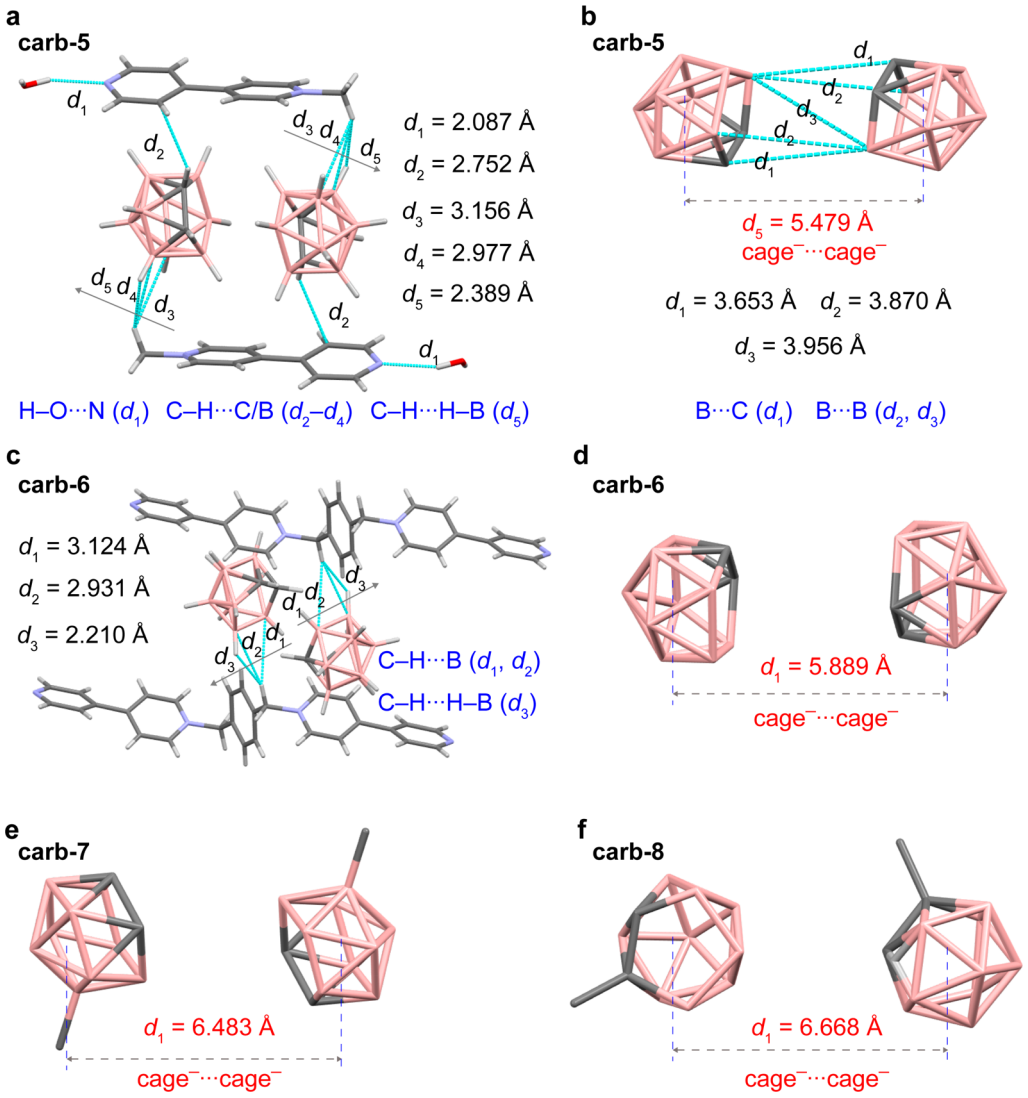

Figure 4. Crystal packing structures of *nido*-carborane-based compounds with different cationic frameworks or *nido*-carboranes with different methyl substitution (blue, nitrogen; dark gray, carbon; pink, boron; light gray, hydrogen; red, oxygen). The contacting distances of the noncovalent bonds are indicated with light blue/black dashed lines. Some hydrogen atoms have been omitted for clarity.

molecular barrier structures. First, if the pyridinium-based molecular barrier in **carb-1** is shortened as shown in compound **carb-5** (Figure 4a), a slightly shorter cage⁻···cage⁻ distance (5.479 Å, Figure 4b) was observed than that in **carb-1** (5.523 Å). Here, O–H···N (2.087 Å), C–H···B/C (2.752–3.164 Å), and C–H···H–B (2.350–2.389 Å) bonds are present in the crystal packing structure (Figure 4a and Figure S7), which contribute to the construction of the restricted lattice environment. The crystallizing water reduces the electron density of the pyridine nitrogen atom through the formation of a hydrogen bond. This further benefits the formation of the cage⁻···cage⁻ interaction. On the contrary, if a longer molecular barrier is chosen as used in compound **carb-6**, multiple intermolecular interactions like C–H···B (2.816–3.186 Å, Figure S8) are observed. Such a packing shape shows a relatively loose packing arrangement between *nido*-carborane and molecular barrier, thus leading to a longer bonding distance of 5.889 Å for the cage⁻···cage⁻ interaction (Figure 4d).

Additionally, the influence of substituent at the *nido*-carborane cage on the cage⁻···cage⁻ interaction was explored as well. In doing so, we designed methyl-substituted *nido*-carboranes at both boron (**carb-7**) and carbon sites (**carb-8**), respectively, but using the same pyridinium-based molecular barrier as in **carb-1**. As expected, the confined space for holding two *nido*-carboranes is also present in **carb-7** (Figure S9). Moreover, the parallel-displaced bonding arrangement still remains but shows longer cage⁻···cage⁻ interaction (6.483 Å, Figure 4e). Consequently, no close C/B···C/B contact of *nido*-carboranes could be observed in this example because of the additional steric hindrance introduced by the methyl group. In the case of **carb-8**, multiple intermolecular interactions such as C–H···B and C–H···H–B were identified (Figure S10). However, because of the larger steric hindrance from the methyl-substituted *nido*-carborane and the orientation, a longer cage⁻···cage⁻ distance of 6.668 Å is generated (Figure 4f). Correspondingly, this leads to an inverse packing orientation of the C_2B_3 planes of the *nido*-carborane units.

Note that **carb-5**, **carb-6**, and **carb-7** contain parallel-displaced cage⁻···cage⁻ interactions and show the common feature of the antisymmetric packing style of two C_2B_3 planes facing each other. Both close and specific contact of the two

https://doi.org/10.1021/jacsau.1c00348
JACS Au 2021, 1, 2047–2057

Scheme 1. Fragmentation Schemes Considered in the Energy Decomposition Analyses[a]

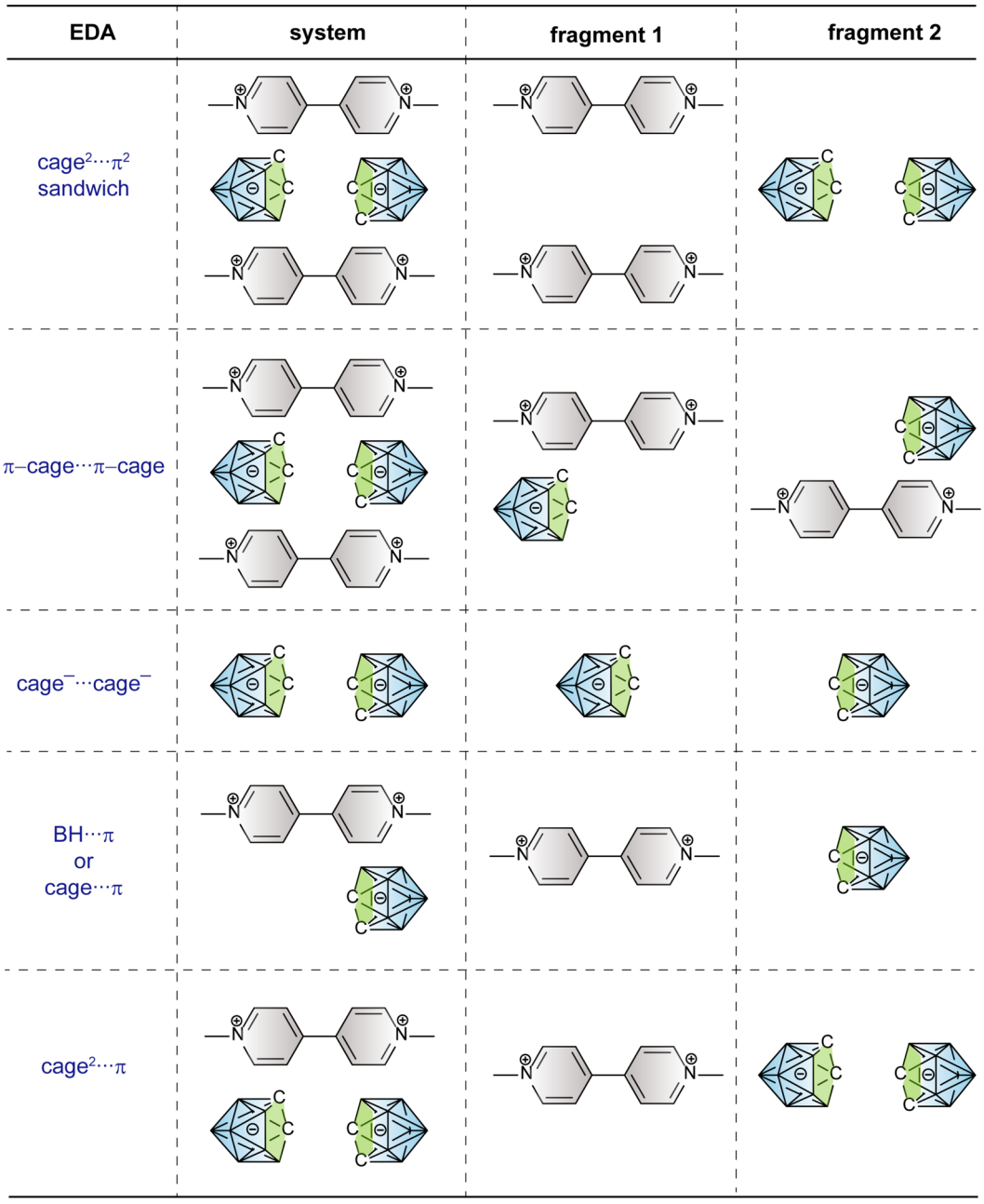

[a]Fragments depicted are based on **carb-1**, although same fragmentation scheme has been applied to the rest of systems. Interactions analyzed for each fragmentation scheme are (1) the interaction between the two three dimensional *nido*-carborane units and the two π-based cations (cage^2···π^2); (2) the cage$^-$···cage$^-$ interaction between the two isolated three dimensional *nido*-$C_2B_9H_{12}$ units (cage$^-$···cage$^-$) and in the presence of two π-based cations (π-cage···π-cage); (3) the cage···π interaction between the three-dimensional *nido*-carborane and the π-based cation (cage···π); (4) the B–H···π interaction between one B–H bond of the carborane and the π-system of one heterocycle (B–H···π); and (5) the interaction between the two three-dimensional *nido*-carborane units and one of the two π-based cations (cage^2···π). Colored in green the C_2B_3 ring and in blue the rest of the carborane cluster.

C_2B_3 planes also suggests effective electronic coupling of the two *nido*-carborane cages. As a whole, noncovalent interactions have been synthetically obtained in boron clusters, which can be tuned by a positively charged molecular barrier.

Energy Decomposition Analysis

The above eight *nido*-carboranes with different cations (**carb-1** to **carb-8**) have been quantum chemically modeled at the ZORA-BLYP-D3BJ/TZ2P level of theory (see the Supporting Information for full computational details). There is a good agreement between computed and crystal packing structures, which have been taken as the initial structures for the molecular structure optimization, as it can be seen from the comparison of the depicted most relevant distances concerning either cage$^-$···cage$^-$, cage···π, and B–H···π interactions or H···H contacts (Figure S11).

The referred interactions presented in this set of structures have been further analyzed by means of a quantitative Kohn–Sham molecular orbital and energy decomposition analysis

https://doi.org/10.1021/jacsau.1c00348
JACS Au 2021, 1, 2047–2057

(EDA) with several fragmentation schemes (Scheme 1). In this EDA, the interaction energy (ΔE_{int}) is decomposed into Pauli (ΔE_{Pauli}), electrostatic (ΔV_{elstat}), orbital interaction (ΔE_{oi}), and dispersion terms (ΔE_{disp}).[64−67]

First, for **carb-1** (Table 1), we found that the cage$^-$···cage$^-$ interaction between the two *nido*-carborane units alone, i.e., without the molecular barrier, is destabilized by 40.3 kcal mol^{-1}, mainly due to the repulsive electrostatic interaction caused by the two anionic systems. However, if the cage$^-$···cage$^-$ interaction is analyzed by enclosing one cation per each carborane, it becomes attractive by −17.2 kcal mol^{-1} (π-cage···π-cage). Thus, the cage$^-$···cage$^-$ interaction becomes "stable" thanks to the presence of the cationic molecular barrier. The main reason is the drastic decrease of the repulsive ΔV_{elstat} term together with more favorable orbital and dispersion interactions due to the formation of B−H···π, C−H···B, or B−H···C noncovalent interactions with the cage and the rings of the cationic units. These interactions (B−H···π or B−H···π') between the cationic ring and the carborane are attractive by −136.4 and −137.8 kcal mol^{-1}, basically due to attractive ΔV_{elstat} between the interacting cation and the anionic cage. The sandwich interaction (cage^2···π^2) between the two *nido*-carboranes together (charge = −2) with the two cationic units together (charge = +4) is attractive by −450.1 kcal mol^{-1}, an interaction fully governed by ΔV_{elstat} (−431.0 kcal mol^{-1}). And finally, the cage^2···π interaction amounts to −255.0 kcal mol^{-1}, somehow larger than half of the sandwich one. From the EDA terms, one can see that the Pauli, the electrostatic, and the dispersion interactions in cage^2···π are halved compared to the sandwich (cage^2···π^2), whereas the orbital interaction remains almost the same. The presence of the second cationic bipyridinium increases, in absolute value, the Pauli, the electrostatic, and the dispersion interactions but does not change the orbital interaction term. Indeed, a similar ΔE_{oi} concurs with similar charge transfer from the cages to the π-based cation(s). Overall, the electrostatic interaction is the most determinant term in all of the above-commented interactions.

Table 1. Energy Decomposition Analysis (kcal mol^{-1}) of the carb-1 *nido*-Carborane-Based Compound Using Different Fragmentation Schemes (Scheme 1)[a]

EDA	ΔE_{Pauli}	ΔV_{elstat}	ΔE_{oi}	ΔE_{disp}	ΔE_{int}	charge[b]
cage^2···π^2	63.2	−431.0	−41.5	−40.8	−450.1	−0.524
π-cage···π-cage	36.1	2.1	−25.0	−30.5	−17.2	−0.524
cage$^-$···cage$^-$	11.2	44.9	−5.7	−10.1	40.3	−1.000
BH···π	16.9	−109.3	−33.6	−10.3	−136.4	−0.305
BH···π'	15.2	−110.3	−32.6	−10.1	−137.8	−0.344
cage^2···π	32.3	−218.1	−48.7	−20.4	−255.0	−0.536

[a]The total VDD charge of the *nido*-carborane in each system is also included (in a.u.). [b]Average charge for different cages of the complexes. [c]See Tables S2−S4 for the rest of the systems.

Systems **carb-3** and **carb-4** (Table S2) present very similar values and trends to **carb-1**. Both **carb-1** and **carb-4** have the two C_2B_3 faces in a parallel but reverse conformation, with face to face distance of 3.83 and 4.13 Å, respectively; whereas in **carb-3** the C_2B_3 rings do not face one to each other. This difference translates into a somewhat less repulsive cage$^-$···cage$^-$ interaction for **carb-3** (37.7 kcal mol^{-1}, Table 1). Finally, **carb-2** (Table S2) presents a completely different conformation, with two more separated carborane units, and just one cationic unit. This translates into a less repulsive cage$^-$···cage$^-$ interaction, due to the longer distance between the two carborane units. And the cage···π interactions appear to be similar to previous B−H···π ones. In a very recent study, the same *nido*-carborane has been analyzed interacting with cationic bipyridiniums, and we have proven the existence of a new *nido*-cage···π noncovalent interaction with similar components of the interaction energy as those of the cage···π interaction in **carb-2**.[47] For completeness, the EDA scheme corresponding to the total dissociation of each system into its fragments, i.e., separate *nido*-carborane clusters and cationic frameworks, has also been undertaken (Table S3), which shows that both initial carborane and pyridinium units experience minor geometry changes when forming the whole compound, with deformation energies (ΔE_{strain}) being in the range of 2.1−7.5 kcal mol^{-1}. The second set of systems, i.e., **carb-5** to **carb-8** (Table S4) provide similar trends and are discussed in the Supporting Information.

It must be also pointed out that the orientation of one *nido*-carborane versus the other one is not determinant, i.e., those with face-to-face orientation like **carb-1** present a similar behavior to those that do not present it, like **carb-3**. Thus, the carborane acts as a whole anionic unit not much influenced by the orientation of the two C_2B_3 rings. This is further supported if we analyze how the bonding energy is affected by changing the packing orientation of the C_2B_3 faces of **carb-1** (Figure S12), with a maximum difference of 8.8 kcal mol^{-1}. In addition, in the case of the same **carb-1**, the increase of distance between the two C_2B_3 faces from the equilibrium distance to that found in other systems causes a relatively small change in the interaction energy (Figure S12). Besides, the methyl group of *nido*-carborane (**carb-7** and **carb-8**) or that in the cationic bipyridinium itself has a minor effect on the electronic properties of these compounds (Figure S13 and Table S5).

Charge Transfer and Molecular Orbital (MO) Interactions

According to Table 1, a charge transfer from the carborane to the cationic aromatic rings of about 0.5 e takes place in **carb-1** (also in **carb-3** and **carb-4**, Table S2). Comparison of the molecular electrostatic potential and VDD charges for the pyridinium and *nido*-carborane systems alone to that of the whole complex clearly shows how the negative charge of the latter is reduced, i.e., transferred to the cationic units, which become less positive (Figure 5 and Figure S14). The reduction of the negative charge in the *nido*-carborane units is particularly important in the C_2B_3 ring (computed QTAIM, Hirshfeld, or Mulliken charges give the same trend, Figures S15 and S16). Thus, the clearly repulsive interaction between the two *nido*-carboranes in the cage$^-$···cage$^-$ fragmentation scheme is drastically reduced by the presence of the cationic framework that acts as a counterion but at the same time efficiently disperses the negative charge of the *nido*-carboranes, as clearly seen in Figure 5. Importantly, from the charge analysis, we can see how the interaction mainly comes through the partially negative hydrogen atoms, i.e., B/C−H$^{\delta-}$···H−C and B−H$^{\delta-}$···π interactions between the cages and the molecular barrier.

Stabilization due to the charge transfer from the anionic *nido*-carborane to the cationic framework is included in the orbital interaction term (ΔE_{oi}). On the basis of the EDA cage^2···π^2 scheme in Table 1 for **carb-1**, the ΔE_{oi} amounts to

https://doi.org/10.1021/jacsau.1c00348
JACS Au 2021, 1, 2047−2057

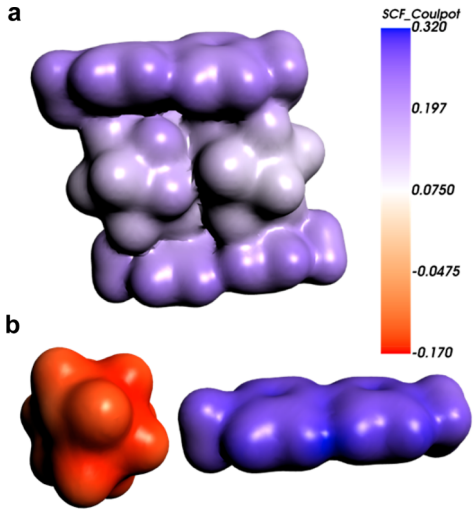

Figure 5. Molecular electrostatic potential isosurfaces for (a) **carb-1** and (b) free *nido*-carborane and cation at the same geometry they have in the whole complex.

−41.5 kcal mol^{-1}. Although ΔE_{oi} is only one tenth of the ΔV_{elstat} term, it is still important for the bonding. EDA analysis supports the relevant HOMO (cage) to LUMO (cation) charge transfer of 0.41 e (Figure S17). The overlap between these HOMO of the carborane and LUMO of the aromatic ring amounts to 0.017.

As a whole, the cage$^-$···cage$^-$ interaction alone is always repulsive. However, such a repulsive interaction can be stabilized by boosting a donor−acceptor interaction with an important charge transfer between the anionic carborane to the cationic aromatic structure. The generated cage$^-$···cage$^-$ bonding interaction as denoted by the π-cage···π-cage fragmentation scheme (Scheme 1 and Table 1), together with the cage···π interaction, is also proven by noncovalent interaction (NCI) plots (Figure S18). Finally, regarding the aromaticity of the C_2B_3 ring, NICS values indicated that it is quite constant along the series (Table S6). Some of us have recently reported[27] that the C_2B_3 ring is not the most aromatic ring in the *nido*-carborane. Indeed, the strongest diatropic ring currents are found in a parallel plane located between the two main five-membered rings of the cluster, i.e., the referred C_2B_3 ring and the B_5 ring below.

Other Aromatic Systems

Would the proposed strategy work for other aromatic anionic species like cyclopentadienyl anion or deprotonated pyrrole? Both systems (Figure S19) have also been analyzed by means of the same procedure as the above series of carboranes, but only using the cationic molecular barrier of **carb-1**. The frontier molecular orbitals of the cyclopentadienyl anion (Cp$^-$) compared to those of the *nido*-carborane (Figure S20) support the similar electronic structure of the two anionic aromatic units. When such a noncovalent interaction is analyzed by means of EDA (Table S7), it is found that the closer distance between the two cyclopentadienyl units as compared to the *nido*-carboranes causes a higher repulsion (ΔE_{int} = 109.5 kcal mol^{-1} for Cp$^-$···Cp$^-$). All terms in absolute value are higher for the two cyclopentadienyl units because of the shorter distance. However, the weight of the different contributions to the final ΔE_{int} remains more or less the same indicating the similarity between the cage$^-$···cage$^-$ and Cp$^-$···Cp$^-$ interactions. The VDD charges also prove the charge transfer from the cyclopentadienyl anion to the cation (Figure S21). Would it be possible to find similar intermolecular interactions in organometallic species? To answer this question, we have considered the dimer of the cyclopentadienylcobalt dicarbonyl complex, $CpCo(CO)_2$. We have found that the dimer with the two Cp units facing each other at 3.560 Å is the most stable. The noncovalent interaction between the two Cp$^-$ units is weak (only 2.9 kcal mol^{-1}), and it is stabilized by the presence of the two units of the cationic $Co^I(CO)_2$ complex (Table S9). These results show that it could be possible to synthesize organic and organometallic aromatic systems with repulsive π^-···π^- noncovalent interactions.

Applications in Solid-State Materials

To explore the properties and potential applications of this new type of cage$^-$···cage$^-$ interaction, a set of experiments were conducted on the selected compound **carb-1** and the model compound **MV** with a bulk-size counteranion of trifluoromethane sulfonimide (Figure 6a). The UV/vis spectra in acetonitrile solution were first investigated. **carb-1** and **MV** showed similar absorption spectra (Figure S24), suggesting no obvious differences in their electronic structures of bipyridinium in the ground state. However, a broad red-shifted absorption was observed for **carb-1** in the crystalline state in comparison to **MV** (Figure 6b). Particularly, it covers the ultraviolet light and the whole visible light ranges, thus might have potential applications in the light-absorbent materials. In sharp contrast, compound **MV** with poor electron donor ability of the trifluoromethane sulfonimide anion showed the short-wavelength absorption band in the solid state (Figure 6b), which is similar to that observed in solution (Figure S24). Thus, the long-wavelength absorption for compound **carb-1** might be attributed to the charge transfer absorption from the donor of *nido*-carborane to the acceptor of bipyridinium. To confirm this, we analyzed the crystal packing structures of the two compounds. Compound **MV** solely shows the O···C and O···N contacts (Figure 6c) between the trifluoromethane sulfonimide anion and bipyridinium cation. In sharp contrast,

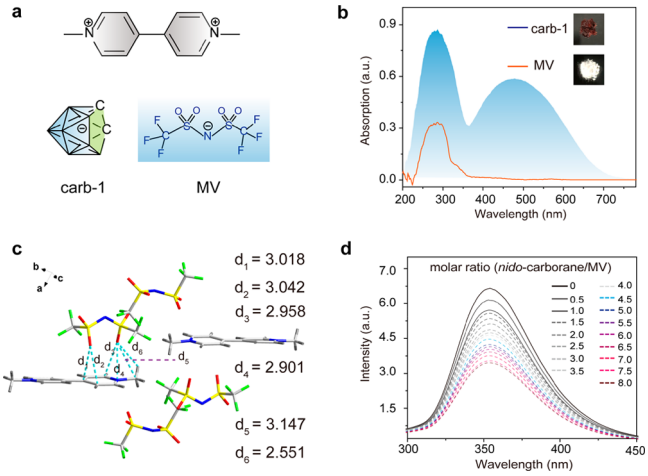

Figure 6. Photophysical properties of compounds **carb-1** and **MV** in the crystalline state. (a) Schemed structures for compounds **carb-1** and **MV**. (b) UV/vis absorption spectra of compounds **carb-1** and **MV** in the solid state. (c) Packing structures of **MV**. (d) PL spectra of the compound **MV** with the addition of *nido*-caborane anion in acetonitrile solution (c = 1.0 × 10^{-5} mol/L, excitation wavelength 260 nm).

https://doi.org/10.1021/jacsau.1c00348
JACS Au 2021, 1, 2047−2057

the compound **carb-1** demonstrates strong interactions between *nido*-carboranes and bipyridinium cation (Figure 3a). Thus, the charge transfer would easily occur, further leading to the long-wavelength absorption in the crystalline state. This also accords with the above theoretical results and is similar to a reported example.[47]

Apart from the above studies, the excited state properties were also investigated. Unexpectedly, compound **carb-1** showed luminescence quenching in the solid state, whereas compound **MV** showed ultraviolet light emission (Figure S25). According to the crystal packing structure, there is no $\pi\cdots\pi$ interaction for compound **carb-1**, which could exclude the excimer-induced quenching effect from the two bipyridinium units. In addition, the ion titration experiment, in which *nido*-carborane-based derivative with a cation of tetramethyl quaternary ammonium was added to the solution of model compound **MV**, displayed a gradually reduced luminous intensity (Figure 6d and Figure S26). Clearly, the charge transfer between *nido*-carborane and pyridinium in the crystal packing structures causes such a luminescence quench in the solid state. As such, the cage$^-\cdots$cage$^-$ interaction-induced packing structure leads to different emission behavior in comparison to the model compound **MV**. Obviously, the boron cluster-based noncovalent bond could be a new supramolecular assembly tool to fine-tune photophysical properties.

Considering the nonemissive nature of **carb-1**, it might devote to maximizing the conversion of light to heat (Figure 7a). Thus, the photothermal conversion of **carb-1** and **MV** crystals was investigated (Figure 7b). The temperature increased very quickly and reached 83 degrees in 1 min of laser irradiation. The efficient photothermal conversion should be attributed to the large absorptivity of **carb-1** molecule as well as the nearly unity efficiency of nonradiative relaxation from the excitons in the excited state (Figure 7a). Such a promising photothermal behavior shows great potential for practical applications.[68] In contrast, control compound **MV** showed a weaker photothermal effect as the temperature increased only to 31°, which may be attributed to the weaker absorption ability and the competing radiation transition of **MV**. Besides, the amorphous **carb-1** sample, having similar ultraviolet absorption as in acetonitrile solution (Figure S24), also shows a negligible photothermal effect (Figures S27−29) compared with that in the crystalline state (Figure 7b). These data demonstrate that the unique packing structures in **carb-1** enable it to show high performance of the photothermal effect. The photobleaching resistance property of **carb-1** was further evaluated by the alternative heating and cooling process, that is, the crystal of **carb-1** was irradiated by laser for 2 min, and then naturally cooled to ambient temperature (Figure 7c). After five cycles, the maximized elevated temperature of **carb-1** showed negligible changes, indicating no degradation under continuous laser irradiation.

Furthermore, the electrical conductivity of **carb-1** and **MV** was measured using an insulation resistance tester on a crystal with a thickness of 1.0 mm (Figure 7d and Figure S30). The conductivity of **carb-1** crystal was determined to be 5.25×10^{-8} S/m at 298 K, which is nearly five times higher than that of control compound **MV**. The enhanced conductivity might be related to the unique packing structures of **carb-1** in the bulk materials. However, such a phenomenon is rarely investigated in carborane-based functional materials.[22−28] According to these results, the boron cluster-based noncovalent interactions endow the bulk crystalline materials with distinct properties, which imparts carborane derivatives with great potential to develop advanced materials.

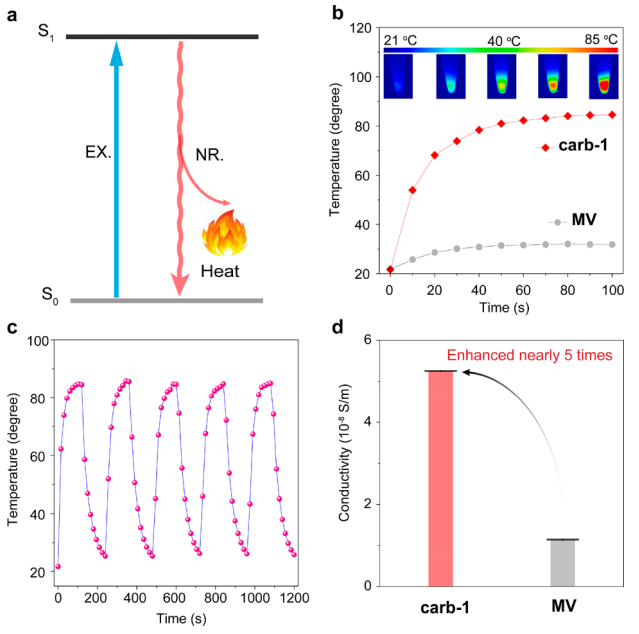

Figure 7. Photothermal and electrical properties of compounds **carb-1** and **MV** in the crystalline state. (a) Decay processes for compound **carb-1** in the excited state. (b) Photothermal conversion of compounds **carb-1** and **MV** under 405 nm laser irradiation and its photothermal images. (c) Photothermal stability study of **carb-1** crystals for five circles of heating−cooling processes. (d) Conductivity measurement for crystals **carb-1** and **MV**.

CONCLUSIONS

In this study, we reported a boron cluster-based noncovalent interaction between two three-dimensional and aromatic *nido*-carborane units, i.e., cage$^-\cdots$cage$^-$ interaction. The nature of this new noncovalent cage$^-\cdots$cage$^-$ bond is electrostatic dominant, mainly supported by B/C−H$^{\delta-}\cdots$H−C and B−H$^{\delta-}\cdots\pi$ interactions between the cages and the cationic pyridinium-based molecular barriers, accompanied by a certain amount of orbital and dispersion interactions. The repulsive interaction between the two *nido*-carboranes is drastically reduced by the presence of the cationic framework that acts as a counterion, while at the same time efficiently dispersing the negative charge of the *nido*-carboranes. The designed carborane derivatives also show interesting properties such as full-color absorption in the crystalline state and efficient photothermal conversion. This work not only provides a new research prospect for carborane chemistry but also offers a paradigm to explore new applications based on boron clusters.

ASSOCIATED CONTENT

Supporting Information

The Supporting Information is available free of charge at https://pubs.acs.org/doi/10.1021/jacsau.1c00348.

Schemes S1−S4 are the chemical structures and the synthetic routes for target compounds in Figures 2 and 3, respectively; Figures S1−S10 and Tables S1 display crystal structures and crystallographic data in this study, respectively; Figures S11−S22 and Tables S2−S8 list

https://doi.org/10.1021/jacsau.1c00348
JACS Au 2021, 1, 2047−2057

computational results not included in the main manuscript; Figures S23−S30 show the physical properties of the compounds in this study; all data supporting the findings of this study are available within the article and its Supporting Information or from the corresponding authors upon reasonable request (PDF)

Crystal structures of carborane-based compounds (CIF)

AUTHOR INFORMATION

Corresponding Authors

Hong Yan − *State Key Laboratory of Coordination Chemistry, Jiangsu Key Laboratory of Advanced Organic Materials, School of Chemistry and Chemical Engineering, Nanjing University, Nanjing 210023, P. R. China;* orcid.org/0000-0003-3993-0013; Email: hyan1965@nju.edu.cn

Jordi Poater − *Departament de Química Inorgànica i Orgànica & Institut de Química Teòrica i Computacional (IQTCUB), Universitat de Barcelona, Barcelona 08028 Catalonia, Spain; ICREA, Barcelona 08010, Spain;* orcid.org/0000-0002-0814-5074; Email: jordi.poater@ub.edu

Miquel Solà − *Institut de Química Computacional i Catàlisi and Departament de Química, Universitat de Girona, Girona 17003 Catalonia, Spain;* orcid.org/0000-0002-1917-7450; Email: miquel.sola@udg.edu

Authors

Deshuang Tu − *State Key Laboratory of Coordination Chemistry, Jiangsu Key Laboratory of Advanced Organic Materials, School of Chemistry and Chemical Engineering, Nanjing University, Nanjing 210023, P. R. China*

Jiaxin Li − *State Key Laboratory of Coordination Chemistry, Jiangsu Key Laboratory of Advanced Organic Materials, School of Chemistry and Chemical Engineering, Nanjing University, Nanjing 210023, P. R. China*

Fangxiang Sun − *State Key Laboratory of Coordination Chemistry, Jiangsu Key Laboratory of Advanced Organic Materials, School of Chemistry and Chemical Engineering, Nanjing University, Nanjing 210023, P. R. China*

Complete contact information is available at: https://pubs.acs.org/10.1021/jacsau.1c00348

Notes

The authors declare no competing financial interest.

ACKNOWLEDGMENTS

This work has been supported by the Ministerio de Economía y Competitividad (MINECO) of Spain (Projects CTQ2017-85341-P, PID2019-106830GB-I00, PID2020-113711GB-I00, and MDM-2017-0767) and the Generalitat de Catalunya (projects 2017SGR39 and 2017SGR348). Excellent service by the Supercomputer center of the Consorci de Serveis Universitaris de Catalunya (CSUC) is gratefully acknowledged. The authors also gratefully acknowledge the financial support from NSFC (21820102004, 21531004, and 91961104).

REFERENCES

(1) Grimes, R. N. *Carboranes*, 3rd ed.; Academic Press: New York, 2016.

(2) Hosmane, N. S. *Boron Science: New Technologies and Applications*; CRC Press: Boca Raton, FL, 2011.

(3) Zhu, Y.; Hosmane, N. S. Liquid-phase synthesis of boron isocyanates: precursors to boron nanoparticles. *Angew. Chem., Int. Ed.* **2018**, *57*, 14888−14890.

(4) Buades, A. B.; Sanchez Arderiu, V.; Olid-Britos, D.; Vinas, C.; Sillanpaa, R.; Haukka, M.; Fontrodona, X.; Paradinas, M.; Ocal, C.; Teixidor, F. Electron accumulative molecules. *J. Am. Chem. Soc.* **2018**, *140*, 2957−2970.

(5) Núñez, R.; Romero, I.; Teixidor, F.; Viñas, C. Icosahedral boron clusters: a perfect tool for the enhancement of polymer features. *Chem. Soc. Rev.* **2016**, *45*, 5147−5173.

(6) Hey-Hawking, E.; Viñas, C., Boron-based compounds. In *Potential and Emerging Applications in Medicine*; Wiley: Chichester, U.K., 2018.

(7) Au, Y. K.; Lyu, H.; Quan, Y.; Xie, Z. W. Copper-catalyzed electrochemical selective B-H oxygenation of *o*-carboranes at room temperature. *J. Am. Chem. Soc.* **2020**, *142*, 6940−6945.

(8) Cui, P. F.; Gao, Y.; Guo, S. T.; Lin, Y.; Li, Z.; Jin, G. X. Metalloradicals supported by a *meta*-carborane ligand. *Angew. Chem., Int. Ed.* **2019**, *58*, 8129−8133.

(9) Naito, H.; Nishino, K.; Morisaki, Y.; Tanaka, K.; Chujo, Y. Solid-state emission of the anthracene-*o*-carborane dyad from the twisted-intramolecular charge transfer in the crystalline state. *Angew. Chem., Int. Ed.* **2017**, *56*, 254−259.

(10) Nghia, N. V.; Jana, S.; Sujith, S.; Ryu, J. Y.; Lee, J.; Lee, S. U.; Lee, M. H. Nido-carboranes: donors for thermally activated delayed fluorescence. *Angew. Chem., Int. Ed.* **2018**, *57*, 12483−12488.

(11) Liu, K.; Shang, C.; Wang, Z.; Qi, Y.; Miao, R.; Liu, K.; Liu, T.; Fang, Y. Non-contact identification and differentiation of illicit drugs using fluorescent films. *Nat. Commun.* **2018**, *9*, 1695.

(12) Kim, T.; Kim, H.; Lee, K.; Lee, Y.; Lee, M. H. Phosphorescence color tuning of cyclometalated iridium complexes by *o*-carborane substitution. *Inorg. Chem.* **2013**, *52* (1), 160−168.

(13) Wee, K.; Han, W.; Cho, D. W.; Kwon, S.; Pac, C.; Kang, S. O. Carborane photochemistry triggered by aryl substitution: carborane-based dyads with phenyl carbazoles. *Angew. Chem., Int. Ed.* **2012**, *51*, 2677−2680.

(14) Ferrer-Ugalde, A.; González-Campo, A.; Viñas, C.; Rodríguez-Romero, J.; Santillan, R.; Farfán, N.; Sillanpää, R.; Sousa-Pedrares, A.; Núñez, R.; Teixidor, F. Fluorescence of new *o*-carborane compounds with different fluorophores: can it be tuned? *Chem. - Eur. J.* **2014**, *20*, 9940−9951.

(15) Scholz, M.; Hey-Hawkins, E. Carbaboranes as pharmacophores: properties, synthesis, and application strategies. *Chem. Rev.* **2011**, *111*, 7035−7062.

(16) Stockmann, P.; Gozzi, M.; Kuhnert, R.; Sárosi, M. B.; Hey-Hawkins, E. New keys for old locks: carborane-containing drugs as platforms for mechanism-based therapies. *Chem. Soc. Rev.* **2019**, *48*, 3497−3512.

(17) Qian, E. A.; Wixtrom, A.; Axtell, J. C.; Saebi, A.; Jung, D.; Rehak, P.; Han, Y.; Moully, E. H.; Mosallaei, D.; Chow, S.; Messina, M. S.; Wang, J. Y.; Royappa, A. T.; Rheingold, A. L.; Maynard, H. D.; Král, P.; Spokoyny, A. M. Atomically precise organomimetic cluster nanomolecules assembled *via* perfluoroaryl-thiol S_NAr chemistry. *Nat. Chem.* **2017**, *9*, 333−340.

(18) Couto, M.; Mastandrea, I.; Cabrera, M.; Cabral, P.; Teixidor, F.; Cerecetto, H.; Viñas, C. Small-molecule kinase-inhibitors-loaded boron cluster as hybrid agents for glioma-cell-targeting therapy. *Chem. - Eur. J.* **2017**, *23*, 9233−9238.

(19) Leśnikowski, Z. J. Challenges and opportunities for the application of boron clusters in drug design. *J. Med. Chem.* **2016**, *59*, 7738−7758.

(20) Zhu, Y.; Hosmane, N. S. Advanced carboraneous materials. *J. Organomet. Chem.* **2017**, *849−850*, 286−292.

(21) Mukherjee, S.; Thilagar, P. Boron clusters in luminescent materials. *Chem. Commun.* **2016**, *52*, 1070−1093.

(22) Williams, R. E. The polyborane, carborane, carbocation continuum: architectural patterns. *Chem. Rev.* **1992**, *92*, 177−207.

(23) Longuet-Higgins, H. G. Substances hydrogénées avec défaut d'électrons. *J. Chim. Phys. Phys.-Chim. Biol.* **1949**, *46*, 268−275.

(24) Eberhardt, W. H.; Crawford, J. B.; Lipscomb, W. N. The valence structure of the boron hydrides. *J. Chem. Phys.* **1954**, *22*, 989−1001.
(25) Lipscomb, W. N. The boranes and their relatives. *Science* **1977**, *196*, 1047−1055.
(26) Poater, J.; Solà, M.; Viñas, C.; Teixidor, F. Aromaticity and three-dimensional aromaticity: two sides of the same coin? *Angew. Chem., Int. Ed.* **2014**, *53*, 12191−12195.
(27) Poater, J.; Viñas, C.; Bennour, I.; Escayola, S.; Solà, M.; Teixidor, F. Too persistent to give up: Aromaticity in boron clusters survives radical structural changes. *J. Am. Chem. Soc.* **2020**, *142*, 9396−9407.
(28) King, R. B. Three-dimensional aromaticity in polyhedral boranes and related molecules. *Chem. Rev.* **2001**, *101*, 1119−1152.
(29) Liu, H.; Zhang, Q.; Wang, M. X. Synthesis, structure, and anion binding properties of electron-deficient tetrahomocorona[4]arenes: shape selectivity in anion-& interactions. *Angew. Chem., Int. Ed.* **2018**, *57*, 6536−6540.
(30) Meyer, E. A.; Castellano, R. K.; Diederich, F. Interactions with aromatic rings in chemical and biological recognition. *Angew. Chem., Int. Ed.* **2003**, *42*, 1210−1250.
(31) Mirzaei, M.; Eshtiagh-Hosseini, H.; Shamsipur, M.; Saeedi, M.; Ardalani, M.; Bauzá, A.; Mague, J. T.; Frontera, A.; Habibi, M. Importance of polarization assisted/resonance assisted hydrogen bonding interactions and unconventional interactions in crystal formations of five new complexes bearing chelidamic acid through a proton transfer mechanism. *RSC Adv.* **2015**, *5*, 72923−72936.
(32) Seth, S. K.; Manna, P.; Singh, N. J.; Mitra, M.; Jana, A. D.; Das, A.; Choudhury, S. R.; Kar, T.; Mukhopadhyay, S.; Kim, K. S. Molecular architecture using novel types of non-covalent f-interactions involving aromatic neutrals, aromatic cations and π-anions. *CrystEngComm* **2013**, *15*, 1285−1288.
(33) Manna, P.; Seth, S. K.; Mitra, M.; Das, A.; Singh, N. J.; Choudhury, S. R.; Kar, T.; Mukhopadhyay, S. A successive layer-by-layer assembly of supramolecular frameworks driven by a novel type of face-to-face π^+-π^+ interactions. *CrystEngComm* **2013**, *15*, 7879−7886.
(34) Geronimo, I.; Lee, E. C.; Singh, N. J.; Kim, K. S. How different are electron-rich and electron-deficient π interactions? *J. Chem. Theory Comput.* **2010**, *6*, 1931−1934.
(35) Mitra, M.; Hossain, A.; Manna, P.; Choudhury, S. R.; Kaenket, S.; Helliwell, M.; Bauzá, A.; Frontera, A.; Mukhopadhyay, S. Melamine-mediated self-assembly of a Cu(II)-methylmalonate complex assisted by π^+-π^+ and anti-electrostatic H-bonding interactions. *J. Coord. Chem.* **2017**, *70*, 463−474.
(36) Eshtiagh-Hosseini, H.; Mirzaei, M.; Zarghami, S.; Bauzá, A.; Frontera, A.; Mague, J. T.; Habibi, M.; Shamsipur, M. Crystal engineering with coordination compounds of 2,6-dicarboxy-4-hydroxypyridine and 9-aminoacridine fragments driven by different nature of the face-to-face aaaaa stacking. *CrystEngComm* **2014**, *16*, 1359−1377.
(37) Chesman, A. S. R.; Hodgson, J. L.; Izgorodina, E. I.; Urbatsch, A.; Turner, D. R.; Deacon, G. B.; Batten, S. R. Anion-anion interactions in the crystal packing of functionalized methanide anions: an experimental and computational study. *Cryst. Growth Des.* **2014**, *14*, 1922−1932.
(38) Zou, W.; Zhang, X.; Dai, H.; Yan, H.; Cremer, D.; Kraka, E. Description of an unusual hydrogen bond between carborane and a phenyl group. *J. Organomet. Chem.* **2018**, *865*, 114−127.
(39) Bhattacharyya, P. B-H_b···π interactions in benzene-borazine sandwich and multidecker complexes: a DFT study. *New J. Chem.* **2017**, *41*, 1293−1302.
(40) Fanfrlík, J.; Pecina, A.; Řezáč, J.; Sedlak, R.; Hnyk, D.; Lepšík, M.; Hobza, P. B-H,: a nonclassical hydrogen bond or dispersion contact? *Phys. Chem. Chem. Phys.* **2017**, *19*, 18194−18200.
(41) Fox, M. A.; Hughes, A. K. Cage C-H···X interactions in solid-state structures of icosahedral carboranes. *Coord. Chem. Rev.* **2004**, *248*, 457−476.
(42) Raston, C. L.; Cave, G. W. V. Nanocage encapsulation of two ortho-carborane molecules. *Chem. - Eur. J.* **2004**, *10*, 279−282.
(43) Frontera, A.; Bauzá, A. *closo*-Carboranes as dual CH-π and BH-π donors: theoretical study and biological significance. *Phys. Chem. Chem. Phys.* **2019**, *21*, 19944−19950.
(44) Sedlák, R.; Fanfrlík, J.; Hnyk, D.; Hobza, P.; Lepšík, M. Interactions of boranes and carboranes with aromatic systems: CCSD(T) complete basis set calculations and DFT-SAPT analysis of energy components. *J. Phys. Chem. A* **2010**, *114*, 11304−11311.
(45) Alkorta, I.; Elguero, J.; Oliva-Enrich, J. M. Hydrogen *vs.* halogen bonds in 1-halo-*closo*-carboranes. *Materials* **2020**, *13*, 2163.
(46) Beau, M.; Lee, S.; Kim, S.; Han, W.-S.; Jeannin, O.; Fourmigué, M.; Aubert, E.; Espinosa, E.; Jeon, I.-R. Strong σ-hole activation on icosahedral carborane derivatives for a directional halide recognition. *Angew. Chem., Int. Ed.* **2021**, *60*, 366−370.
(47) Tu, D. S.; Yan, H.; Poater, J.; Solà, M. The *nido*-cage···π bond: a non-covalent interaction between boron clusters and aromatic rings and its applications. *Angew. Chem., Int. Ed.* **2020**, *59*, 9018−9025.
(48) Sivaev, I. B.; Bregadze, V. V. Polyhedral boranes for medical applications: current status and perspectives. *Eur. J. Inorg. Chem.* **2009**, *2009*, 1433−1450.
(49) Zhao, L. L.; Hermann, M.; Schwarz, W. H. E.; Frenking, G. The Lewis electron-pair bonding model: modern energy decomposition analysis. *Nature Rev. Chem.* **2019**, *3*, 48−63.
(50) Deng, G.; Pan, S.; Wang, G.; Zhao, L.; Zhou, M.; Frenking, G. Side-on bonded beryllium dinitrogen complexes. *Angew. Chem., Int. Ed.* **2020**, *59*, 10603−10609.
(51) Hawthorne, M. F. The chemistry of the polyhedral species derived from transition metals and carboranes. *Acc. Chem. Res.* **1968**, *1*, 281−288.
(52) Masalles, C.; Llop, J.; Viñas, C.; Teixidor, F. Extraordinary overoxidation resistance increase in self-doped polypyrroles by using non-conventional low charge-density anions. *Adv. Mater.* **2002**, *14*, 826−829.
(53) Mata, I.; Alkorta, I.; Molins, E.; Espinosa, E. Electrostatics at the origin of the stability of phosphate-phosphate complexes locked by hydrogen bonds. *ChemPhysChem* **2012**, *13*, 1421−1424.
(54) Mata, I.; Alkorta, I.; Molins, E.; Espinosa, E. Tracing environment effects that influence the stability of anion-anion complexes: The case of phosphate-phosphate interactions. *Chem. Phys. Lett.* **2013**, *555*, 106−109.
(55) Mata, I.; Molins, E.; Alkorta, I.; Espinosa, E. The paradox of hydrogen-bonded anion-anion aggregates in oxoanions: a fundamental electrostatic problem explained in terms of electrophilic··· nucleophilic interactions. *J. Phys. Chem. A* **2015**, *119*, 183−194.
(56) Alkorta, I.; Mata, I.; Molins, E.; Espinosa, E. Charged versus neutral hydrogen-bonded complexes: is there a difference in the nature of the hydrogen bonds? *Chem. - Eur. J.* **2016**, *22*, 9226−9234.
(57) Lamberts, K.; Handels, P.; Englert, U.; Aubert, E.; Espinosa, E. Stabilization of polyiodide chains *via* anion···anion interactions: experiment and theory. *CrystEngComm* **2016**, *18*, 3832−3841.
(58) Daolio, A.; Pizzi, A.; Terraneo, G.; Ursini, M.; Frontera, A.; Resnati, G. Anion···anion coinage bond: the case of tetrachloridoaurate. *Angew. Chem., Int. Ed.* **2021**, *60*, 14385−14389.
(59) He, Q.; Tu, P.; Sessler, J. L. Supramolecular chemistry of anionic dimers, trimers, tetramers, and clusters. *Chem.* **2018**, *4*, 46−93.
(60) Wang, H.; Fang, S.; Wu, G.; Lei, Y.; Chen, Q.; Wang, H.; Wu, Y.; Lin, C.; Hong, X.; Kim, S. K.; Sessler, J. L.; Li, H. Constraining homo- and heteroanion dimers in ultraclose proximity within a self-assembled hexacationic cage. *J. Am. Chem. Soc.* **2020**, *142*, 20182−20190.
(61) He, Q.; Kelliher, M.; Bähring, S.; Lynch, V. M.; Sessler, J. L. A bis-calix[4]pyrrole enzyme mimic that constrains two oxoanions in close proximity. *J. Am. Chem. Soc.* **2017**, *139*, 7140−7143.
(62) Mantina, M.; Chamberlin, A. C.; Valero, R.; Cramer, C. J.; Truhlar, D. G. Consistent van der Waals Radii for the whole main group. *J. Phys. Chem. A* **2009**, *113*, 5806−5812.

https://doi.org/10.1021/jacsau.1c00348
JACS Au 2021, 1, 2047−2057

(63) Hunter, C. A.; Sanders, J. K. M. The nature of π-π interactions. *J. Am. Chem. Soc.* **1990**, *112*, 5525−5534.
(64) Bickelhaupt, F. M.; Diefenbach, A.; de Visser, S. P.; de Koning, L. J.; Nibbering, N. M. M. Nature of the three-electron bond in $H_2S.^{\cdot}.SH_2^+$. *J. Phys. Chem. A* **1998**, *102*, 9549−9553.
(65) Bickelhaupt, F. M.; Baerends, E. J. *Reviews in Computational Chemistry*; Lipkowitz, K. B., Boyd, D. B., Eds.; Wiley−VCH: New York, 2000; Vol. *15*, pp 1−86.
(66) Wolters, L. P.; Bickelhaupt, F. M. The activation strain model and molecular orbital theory. *WIRES Comput. Mol. Sci.* **2015**, *5*, 324−343.
(67) Hopffgarten, M. V.; Frenking, G. Energy decomposition analysis. *Wiley Interdiscip. Rev.: Comput. Mol. Sci.* **2012**, *2*, 43−62.
(68) Xi, D.; Xiao, M.; Cao, J.; Zhao, L.; Xu, N.; Long, S.; Fan, J.; Shao, K.; Sun, W.; Yan, X.; Peng, X. NIR light-driving barrier-free group rotation in nanoparticles with an 88.3% photothermal conversion efficiency for photothermal therapy. *Adv. Mater.* **2020**, *32*, 1907855.

https://doi.org/10.1021/jacsau.1c00348
JACS Au 2021, 1, 2047−2057